WATER RESOURCES RESEARCH, VOL. 46, W05601, doi:10.1029/2008WR007672, 2010

Near real-time flood wave approximation on large rivers from space: Application to the River Po, Italy

G. Schumann,[1] G. Di Baldassarre,[2] D. Alsdorf,[3] and P. D. Bates[1]

Received 19 December 2008; revised 14 December 2009; accepted 30 December 2009; published 18 May 2010.

[1] This paper investigates the potential of low-cost spaceborne data to approximate longitudinal surface profiles during flood events on large rivers. In February 2000, the Shuttle Radar Topography Mission (SRTM) measured the elevation of most of the Earth's surface with spatially continuous sampling and an absolute vertical accuracy between 5.6 and 9 m. The vertical error has been shown to change with topographic complexity, being less important over flat terrain. This allows water surface slopes to be measured and associated discharge volumes to be estimated for open channels in large basins, such as the Amazon. Building on these capabilities, this paper demonstrates that near real-time coarse resolution radar imagery of a recent flood event on a 98 km reach of the River Po (Italy) combined with SRTM terrain height data leads to a water slope remarkably similar to that derived by combining the radar image with highly accurate airborne laser altimetry. Moreover, it is shown that this spaceborne flood wave approximation compares well to a hydraulic model and thus allows the performance of the latter, calibrated on a previous event, to be assessed when applied to an event of different magnitude in near real time. These results are not only of great importance to real-time flood management and flood forecasting but also support the upcoming Surface Water and Ocean Topography mission that will routinely provide water levels and slopes with higher precision around the globe.

Citation: Schumann, G., G. Di Baldassarre, D. Alsdorf, and P. D. Bates (2010), Near real-time flood wave approximation on large rivers from space: Application to the River Po, Italy, *Water Resour. Res.*, *46*, W05601, doi:10.1029/2008WR007672.

1. Introduction

[2] Flooding accounts for about 40% of all natural hazards worldwide and half of all deaths caused by natural disasters [e.g., *Ohl and Tapsell*, 2000; *Jonkman and Vrijling*, 2008]. Moreover, the recent major floods in Europe, such as the catastrophic central European flooding in 2002 and the UK flash flooding in 2004 and 2007, triggered the widespread perception that flood risk in Europe is increasing [e.g., *European Environment Agency*, 2005; *Wilby et al.*, 2008].

[3] Hydraulic models which reproduce the hydraulic behavior of river channels and floodplains have proven to be useful tools in floodplain management [*Horritt et al.*, 2007] as well as flood risk assessment [e.g., *Merz et al.*, 2007]. Specifically, several applications of hydraulic engineering (e.g., design analysis and maintenance of embankments) require the reconstruction of historical flood water levels and approximation of waves over the event duration. Given that spatially distributed level observations are rarely available, this is usually achieved by simulating events with flood inundation models. It is well known that models are affected by errors and uncertainties that depend on the particular model used, test site and quality of topographic and hydrologic data. Moreover, it is important to note that even in the fortunate case in which a model can be calibrated on previous flood events, it may still give a poor prediction for events of different magnitude. In fact, several studies [e.g., *Aronica et al.*, 1998; *Horritt and Bates*, 2002; *Romanowicz and Beven*, 2003; *Horritt et al.*, 2007; *Pappenberger et al.*, 2007] have shown that effective model parameters (i.e., roughness coefficients) differ when evaluated for flood events of different magnitude.

[4] Observed water level and flood extent data are therefore critical to constraining the predictions of flood inundation models. Water levels are typically obtained from either in-channel gaging stations or reflectorless total stations [e.g., *Pasternack et al.*, 2008]. Also, sonar boats equipped with GPS using real time kinematic (RTK) satellite navigation to provide real-time corrections to a centimeter level of accuracy [*Shields et al.*, 2003] or even satellite profiling altimeters [*Frappart et al.*, 2006; *Alsdorf et al.*, 2007b] to cover larger areas might be used. The process can also be facilitated by the placement of stage markers followed by surveying after the event at one's convenience. Coherent pairs of radar images can also be processed interferometrically to yield maps of water level change [*Alsdorf et al.*, 2000, 2007a]; however, this is only possible over flooded vegetation where a double bounce allows a signal to be returned to the sensor. Flood extents can be mapped conducting field surveys during the event or from postevent wrack marks using handheld GPS and from aerial photography, satellite imaging radars [*Schumann et al.*, 2009] or optical spaceborne sensors [*Marcus and Fonstad*, 2008]. Flood extents from imagery can also be intersected with high-resolution digital terrain models

[1]School of Geographical Sciences, University of Bristol, Bristol, UK.
[2]Department of Hydroinformatics and Knowledge Management, UNESCO-IHE, Delft, Netherlands.
[3]School of Earth Sciences, Ohio State University, Columbus, Ohio, USA.

0043-1397/10/2008WR007672

Table 1. Current Satellite Missions Featuring High-Resolution SAR Sensors With High Potential for Flood Studies[a]

Mission (Agency: Year of Launch)	Band: λ	Polarization	Spatial Resolution (m)	Repeat Cycle[b] (days)
ERS-2 (ESA: 1995)	5.3 GHz (C: 5.6 cm)	VV	25	35
RADARSAT-1 (CSA: 1995)	5.3 GHz (C: 5.6 cm)	HH	8–100	24
ENVISAT (ESA: 2002)	5.3 GHz (C: 5.6 cm)	VV-VH, VV-HV	12.5–1000	35
ALOS (JAXA: 2006)	1.3 GHz (L: 23.6 cm)	full	7–100	46
COSMO-SkyMed[c] (ASI: 2007)	9.6 GHz (X[d]: 3.1 cm)	dual	15–100	16
TerraSAR-X (DLR: 2007)	9.6 GHz (X: 3.1 cm)	full	1–16	11
RADARSAT-2 (MDA: 2007)	5.3 GHz (C: 5.6 cm)	full	3–100	24

[a]Operating agency, year of launch, sensor frequency, mode of polarization, spatial resolution, and repeat cycle are also shown [*Schumann et al.*, 2009].
[b]At highest spatial resolution. There is a strong inverse relationship between spatial resolution and repeat cycle (e.g., for RADARSAT-1 a daily repeat cycle is possible with a spatial resolution of 100 m). However, it is worth bearing in mind that timely acquisition can be programmed (tasked) for all satellites in case of emergency (usually 24–48 h advance notice is required).
[c]This is a constellation of four SAR satellites operated by ASI and the Italian military. Although the orbit repeat cycle is 16 days, the constellation allows a very fast response time of only several hours.
[d]Multiband (X, C, L, P) sensors are planned for the future.

(DTMs), particularly from airborne laser altimetry (LiDAR), to enable the extraction of water heights at the shoreline [*Schumann et al.*, 2007; *Mason et al.*, 2007; *Hostache et al.*, 2009]. Accounting for flood mapping and related uncertainties across entire floodplain sections perpendicular to the flow direction has enabled this technique to be augmented by estimations of uncertainties associated with shoreline heights and approximation of water surface gradients thereof [*Schumann et al.*, 2008b].

[5] A key problem with all the above data sets are their limited spatial and temporal coverages. During flood events, optical satellite imagery is most of the time obstructed by persistent cloud cover. Field-based mapping techniques are highly accurate (with errors commonly <10 cm) but usually lack the desired spatial coverage and are difficult to carry out during flood events. In-channel gaging stations and profiling altimeter tracks are widely spaced (10–120 km), and the latter requires large water widths (>1 km) to accurately retrack water levels [*Birkett et al.*, 2002]. High-resolution radar imagery or aerial photography of floods are only ever acquired opportunistically, and high-quality data are consequently only available at a limited number of sites globally given the low orbit revisit times (35 days for ERS, 7–10 days for RADARSAT) of typical sensors (Table 1). Moreover, very few of the sites where good quality imagery are available also have high-resolution DTM data (such as from LiDAR) to permit extraction of shoreline heights and even fewer have emergent vegetation that would allow interferometric analysis. Acquiring high-resolution radar and DTM data can also incur considerable costs, and existing data may be subject to copyright restrictions. Nevertheless flood inundation is a global hazard, and if low-cost and timely water level data could be shown to have value for hydraulic model calibration then the number of sites where models can be developed may be substantially increased. The trade-off to achieve global and/or more frequent coverage is that more use will likely need to be made of lower-accuracy and lower-resolution data than have so far been applied in model validation studies.

2. Study Objective

[6] In this paper we investigate the feasibility of using freely available, low-accuracy digital elevation models derived from the Shuttle Radar Topography Mission (SRTM) at a geometric resolution of 3 arc seconds (≈90 m) combined with low-resolution wide swath imagery, both available in near real time (NRT, ≤24 h after image acquisition), to approximate a water surface profile from space. With a typical 400 km image swath width for a spatial ground resolution of 150 m (pixel spacing: 75 m) any area can be revisited more frequently than can be achieved with most existing satellites, permitting an improved temporal sampling. Only very few studies so far have demonstrated the potential of SRTM data to derive useful hydraulic parameters, such as water surface slope and discharge [*LeFavour and Alsdorf*, 2005; *Kiel et al.*, 2006; *Wang et al.*, 2005; *Schumann et al.*, 2008a], and none of these studies have validated the derived water surface gradients or profiles or used them to evaluate hydraulic model predictions.

[7] To complement and extend previous work, we illustrate the use of SRTM and low-resolution radar imagery acquired by the ENVISAT satellite to approximate flood wave profiles on large rivers (with a floodplain width >500 m to accommodate the lower spatial resolution of wide swath imagery with a pixel size ≥75 m; for more details on flood extent mapping and spatial resolution requirements, see *Blyth* [1997]) adequately in NRT. The study is conducted using a low-resolution radar image of a flood in late spring 2008 on a 98 km reach of the River Po in Italy. Results are compared to an equivalent flood wave profile determined using the low-resolution radar image and LiDAR data. Moreover, the paper attempts to evaluate the potential of low-cost spaceborne data to support hydraulic modeling. It is expected that the findings will be of great benefit to global flood forecasting and management as well as providing support for existing proof-of-concept studies for the upcoming Surface Water and Ocean Topography (SWOT) mission based on the SRTM heritage (http://swot.jpl.nasa.gov/).

3. Test Site, Available Data, and Hydraulic Modeling

3.1. Test Site and Data

[8] The reach of the River Po is located between the two gaging stations of Cremona and Borgoforte (Figure 1). For this portion of the river, the riverbed consists of a stable main channel with a width equal to about 250 m and two lateral floodplains, with an overall width variable from 400 m to 4 km, confined by two continuous artificial embankments.

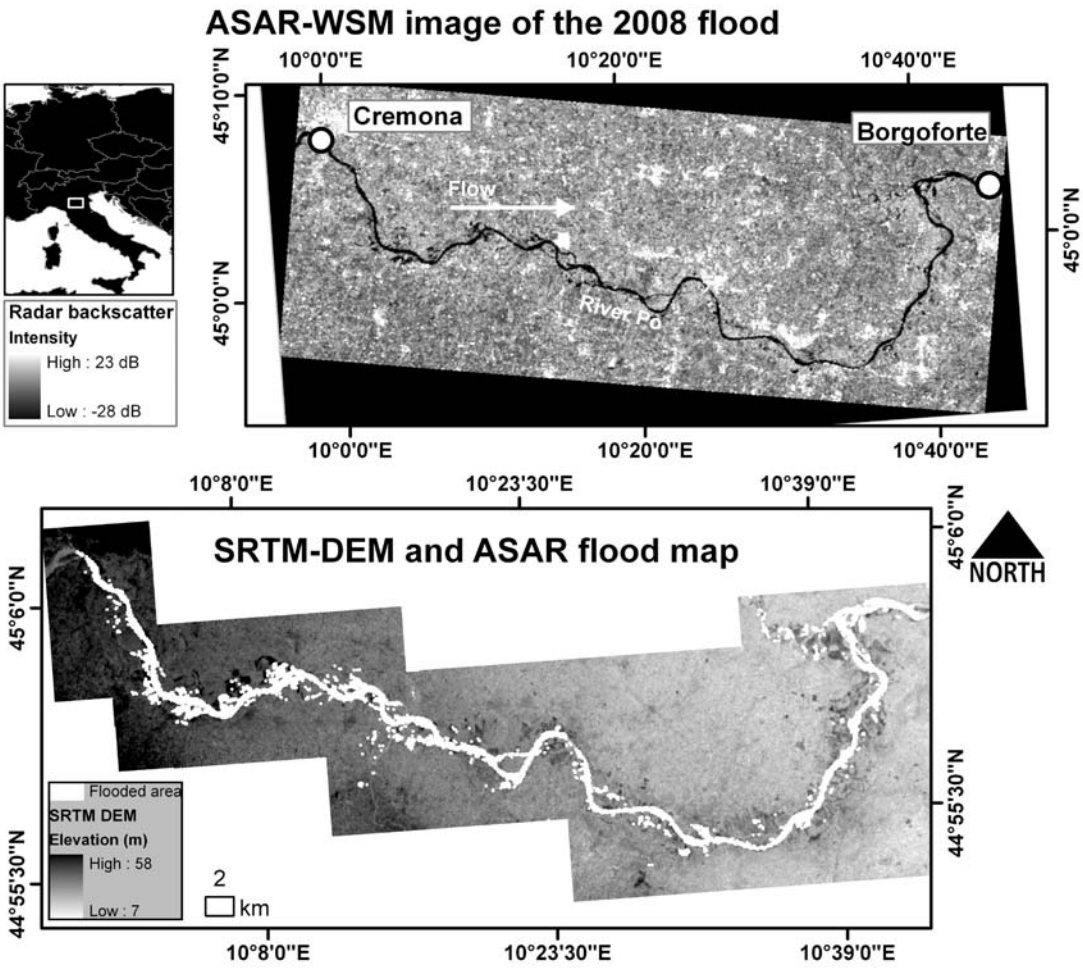

Figure 1. The 98 km test reach of the River Po between Cremona and Borgoforte (Italy). The ASAR-derived flood area and SRTM DEM are shown. Data provided by the European Space Agency.

[9] Between the end of May and the beginning of June 2008 the River Po experienced a low-magnitude flood event of 5736 m^3s^{-1} with a return period equal to about 2 years [*Di Baldassarre et al.*, 2009], for which no field data were collected. However, on the 1st of June at 9:26 a.m., about 1 h before the peak flow at Cremona, coarse resolution wide swath SAR imagery with a ground resolution of <150 m was acquired and processed (Figure 1). The flood image, provided through the Fast Registration system of the European Space Agency (ESA) at no cost 24 h after acquisition, is a C band Advanced SAR image in Wide Swath Mode (ASAR WSM) with a VV polarization. Due to the wide swath of the image this acquisition mode provides very frequent coverage (≈ every 3 days) and is thus very well suited for flood monitoring on larger rivers for which flood wave travel time would be >1 day.

[10] The River Po Basin Authority recently commissioned the construction of a 2 m LiDAR DTM of a 350 km reach of the middle-lower portion of the River Po. Below the water surface, channel bathymetry of the navigable portion was acquired during the same year (2005) by boat surveying using multibeam sonar. Elsewhere, these data were supplemented with ground survey of cross sections conducted by AIPO (Interregional Authority of the River Po).

3.2. Hydraulic Modeling

[11] As noted earlier, we also investigated the ability of low-resolution remote sensing to verify water levels from hydraulic models. In order to reconstruct the June 2008 flood, the UNET 1-D hydraulic code [*Barkau*, 1996], available as part of the software package HEC-RAS [*U.S. Army Corps of Engineers*, 2002], was used. The code solves the de St-Venant equations with an algorithm based on the Preissmann implicit four-point finite difference scheme [*Preissmann*, 1961]. The model is built by using 88 cross sections (even spacing: about 1 km) extracted from the high-quality LiDAR DTM and the bathymetric data. The cross-section spacing is derived using guidance reported in the scientific literature [*Samuels*, 1990; *Castellarin et al.*, 2009]. The observed flow hydrograph at the upstream end and the observed water levels at the downstream end define the model boundary conditions.

[12] As no data other than the ASAR WSM imagery and a gaged water level at both reach ends are available for the 2008 event, this model was calibrated on an event in 2000 (HEC-RAS A) for which extensive field data exist. Calibration was achieved by minimizing the difference between simulated maximum water elevation and 176 high water marks on the two banks surveyed in the aftermath of the October 2000

high-magnitude flood event [*Di Baldassarre et al.*, 2009], which had an estimated peak discharge of approximately 12000 m^3s^{-1} corresponding to a return period of about 60 years [*Maione et al.*, 2003]. Given the homogeneous characteristics of the river reach, it was found to be sufficient to limit the potentially distributed Manning's *n* parameters to one value for the channel and one for the floodplain. The performance of the best fit calibration for the 2000 event (with Manning's *n* coefficients of 0.04 $m^{1/3}s^{-1}$ for the channel and 0.09 $m^{1/3}s^{-1}$ for the floodplain) is very high for all cross sections with a mean absolute error between observed and simulated water levels equal to 0.24 m (relative error equal to 1%). *Di Baldassarre et al.* [2009] performed an internal verification and subsequent recalibration of the model for the 2008 event using absolute inundation width derived from the ASAR image (HEC-RAS B, with Manning's *n* coefficients of 0.02 $m^{1/3}s^{-1}$ for the channel and 0.05 $m^{1/3}s^{-1}$ for the floodplain). The analysis pointed out that the 2000 event calibration, although able to reproduce the high-magnitude flood with excellent results, is inappropriate as it fails to reproduce the low-magnitude flood event of June 2008, as might be expected.

[13] Given the absence of field-based water levels in 2008, we use both the 2000 and the 2008 calibrated models (HEC-RAS A and B, respectively) to assess the validity of the remote sensing water levels and the ability to distinguish between competing model parameterizations. By doing so, we believe it is fair to assume that the absolute inundation width is a different parameter to the water levels we derive here.

4. Methods: Flood Wave Approximation Using Spaceborne Sensors

4.1. Accounting for Uncertainties

[14] It is now widely appreciated that flood area can be successfully mapped from spaceborne SAR [*Smith*, 1997; *Schumann et al.*, 2009], although uncertainties in mapping procedures and in flood edge positioning are considerable and therefore worth accounting for [e.g., *Schumann et al.*, 2008b; *Hostache et al.*, 2009]. The ASAR was received geolocated to within one pixel accuracy. Further investigation using independent check points (ICPs) at bridge locations revealed a mean error of 56.5 m and a standard deviation of 34.5 m; the RMS pixel error is 64.4 m.

[15] Extracting flooded areas from a radar image of low spatial resolution often results in scattered flood patches (Figure 1). Therefore, accounting for all uncertainties in extent positioning as much as possible when extracting heights from a DEM at the flood edges seems sensible. In fact, *Schumann et al.* [2008b] have shown that extracting heights at the flood edges assuming a horizontal level at each individual flood patch (resulting mostly from image processing and geolocation uncertainties in the case of LiDAR) across equally spaced river cross sections drawn perpendicular to the stream centerline gives an appreciation of water level uncertainty perpendicular to the flow, in addition to downward trends in flow direction. Furthermore, numerous data points on individual river sections increase the credibility of a best fit line to represent the water surface gradient, as the regression model is conditioned on more data points. This approach is adopted here and applied to the ASAR WSM image and SRTM DEM with the aim to investigate the potential of coarse resolution spaceborne remote sensing to adequately approximate flood wave profiles on large rivers in NRT. The procedure to account for the errors inherent in flood edge positioning and height when estimating water levels from radar imagery is described by *Schumann et al.* [2008b] and is summarized hereafter.

[16] Flood edge positioning errors result primarily from inaccurate geolocation and inherent uncertainties in the chosen extraction algorithm. As noted above, we used ICPs to compute the geolocation error. In terms of flood extraction, we computed a global threshold value from the (gray level) histogram of the radiometrically corrected WSM image (i.e., actual backscatter) using Otsu's method [*Otsu*, 1979]. The threshold was then applied to the image to generate a binary flood map showing wet and dry pixels. Otsu's method applies a criterion measure to evaluate the between-class variance (i.e., separability) of a threshold at level k computed from an image histogram of L gray levels. The objective function is given by:

$$\eta(k) = \frac{\sigma_B^2(k)}{\sigma_T^2} \tag{1}$$

where σ_B^2 is a function of threshold level k based on class means, while σ_T^2 denotes total variance and is independent of k. The optimal threshold k^* that maximizes η, or equivalently maximizes σ_B^2 is selected during a sequential search and is

$$\sigma_B^2(k^*) = \max_{1 \le k < L} \sigma_B^2(k) \tag{2}$$

[17] We used the distance between η and its maximum of 1, which is attainable only by two-valued images, as an index for the uncertainty in defining k^*. For the WSM image, the position of k^* on the image histogram could vary by 0.14. This translates into a possible maximum flood edge between a backscatter value of −13.4 and −8.5 dB, with η optimized at −11 dB (k^*). For ease of processing, we decided to classify every value below −8.5 dB (i.e., the highest backscatter intensity in this range) as flooded (Figure 1), although a weighting scheme with a maximum at k^* might be used.

[18] Apart from the horizontal uncertainty, there is the vertical component that might have a considerable impact on water level accuracy, particularly in the case of SRTM with an absolute vertical accuracy between 5.6 and 9 m across the globe [*Farr et al.*, 2007]. This vertical error has been shown to be correlated with topographic relief with large errors and data voids over high-relief terrain while in the low-relief sites errors are smaller but still affected by hilly terrain [*Falorni et al.*, 2005]. For our study site, a comparison with LiDAR heights across the Po floodplain revealed a mean error of −0.47 m. Although here we corrected for this half a meter bias (assuming the LiDAR has no error), it is worth noting that given the normal distribution of residuals (paired t test p: 0.98), it can be assumed that not accounting for the vertical bias in SRTM (in case no other height source is available) would lower a regression model estimation by only 0.47 m on average. After bias correction, the standard deviation is 2.95 m. This relatively good performance of the SRTM data is to be expected given the very flat topography of the reach; but is assumed to be of a similar order in other floodplains around the globe. It is noteworthy that although the mean

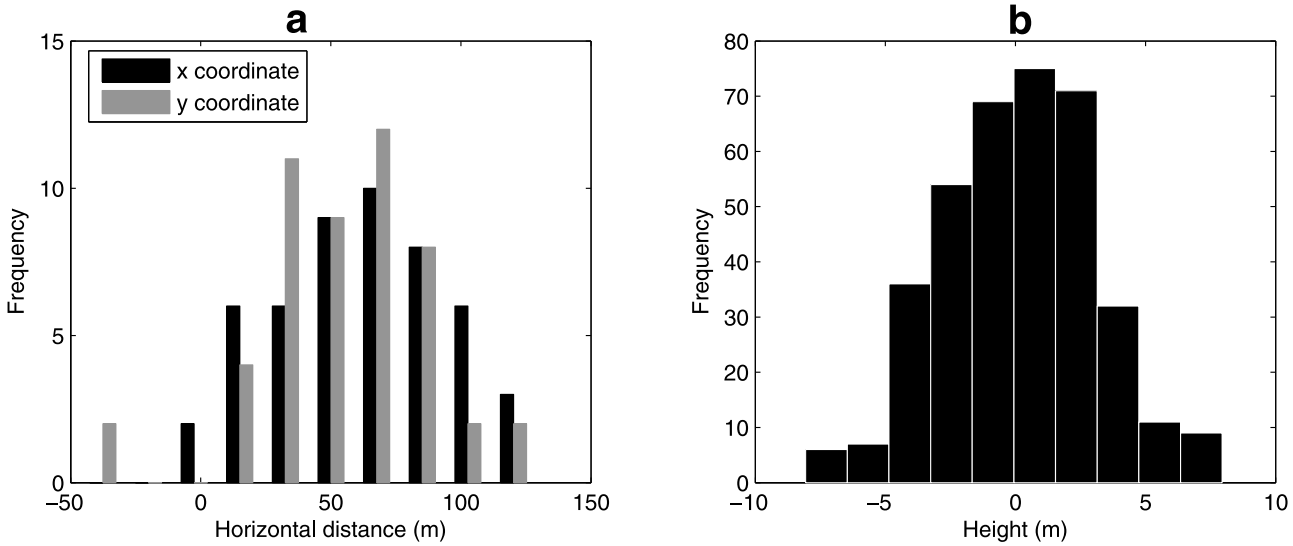

Figure 2. Distributions of errors for (a) the geolocation (x, y coordinates) of the flood edge (i.e., horizontal component) and (b) the height of the flood edge (i.e., vertical component). A total of 50 x, y pairs were generated for the horizontal component; each pair being applied to every flood edge position in the entire image, thus resulting in multiple image shifts.

error might be used to adjust SRTM heights, the aim of this analysis is rather to add random vertical errors in order to account for all possible sources of error.

[19] Using the mean error and standard deviation, we sampled normally distributed errors for the horizontal (flood edge positioning) and vertical (height) uncertainty source (Figure 2) that we added to the processed flood edge x and y coordinate positions and flood edge heights, respectively, in order to account for possible errors related to the entire processing chain.

4.2. Estimating a Water Surface Slope and Levels

[20] For SRTM data, *LeFavour and Alsdorf* [2005] found that reliable slopes may only be obtained when reach lengths extend sufficient distances to accommodate the height errors inherent in the SRTM elevation returns over open water surfaces. The appropriate reach length can be obtained with equation (3). Assuming that elevations along water surfaces are expected to have little variation, *LeFavour and Alsdorf* [2005] concluded that, after removal of the linear trend, the standard deviation (σ) is a strong indicator of height error for a given reach. Note that in this study we not only use the SRTM returns from the (permanent) water surface but also the returns from the land flooded on the satellite image; however the same principle should hold. By also using returns from the inundated floodplain, we assume that the water surface slope is different to the valley slope (which was shown to be at least 0.6 m by the gaged data). For the investigated reach of the River Po, σ is 4.5 m after detrending and the river gradient, $S_{\min}$, is 0.16 m km^{-1}, which gives a minimum reach length of 56 km using equation (3).

$$RL = \frac{2\sigma}{S_{\min}} \tag{3}$$

[21] So the investigated reach length of 98 km is sufficient to estimate the surface water slope and should thus allow us to obtain an adequate approximation of the flood wave profile for the 2008 event, in NRT. The accuracy of this profile will be assessed by comparing it to the profile obtained with LiDAR data.

5. Results and Discussion

[22] Accounting for as many errors as possible during the processing chain resulted in quite a large spread of likely water level estimations at each river cross section (Figure 3a). Although the spread might be significantly large, statistical measures can now be derived for each cross section. It is expected that regression modeling performed on all these data points results in a reliable approximation of a water surface slope and levels [*Schumann et al.*, 2008b].

[23] Indeed, fitting a third-order polynomial through the SRTM heights extracted for each river section at the flood edges, assuming a horizontal level at each individual flood patch (Figure 3a), gives an approximation of the longitudinal profile of the flood wave at the time of image acquisition. It is worth noting that for more natural basins such as the Amazon water levels in the floodplain might be very different to those in the river [*Alsdorf et al.*, 2007a] and thus a conventional hydraulic 1-D or quasi 1-D approximation as adopted here would probably be inappropriate. Mostly as a result of the low-resolution ASAR image, the best fit line for the SRTM is also remarkably similar to that obtained when a very high quality airborne LiDAR system (Figures 3b and 3c) is used to generate the DEM (mean elevation error: −26 cm). Whilst the spread around the best fit line is much larger in the case of SRTM, the process still results in a respectable R^2 value (coefficient of determination for SRTM: 0.63, LiDAR: 0.86). Figure 3c illustrates that the confidence intervals based on residuals overlap but are wider in the case of SRTM, as expected. We also wish to highlight that not adding random height errors changes the mean elevation error between LiDAR and SRTM only by 3 cm, although this is expected to be much more significant for more heterogeneous floodplains

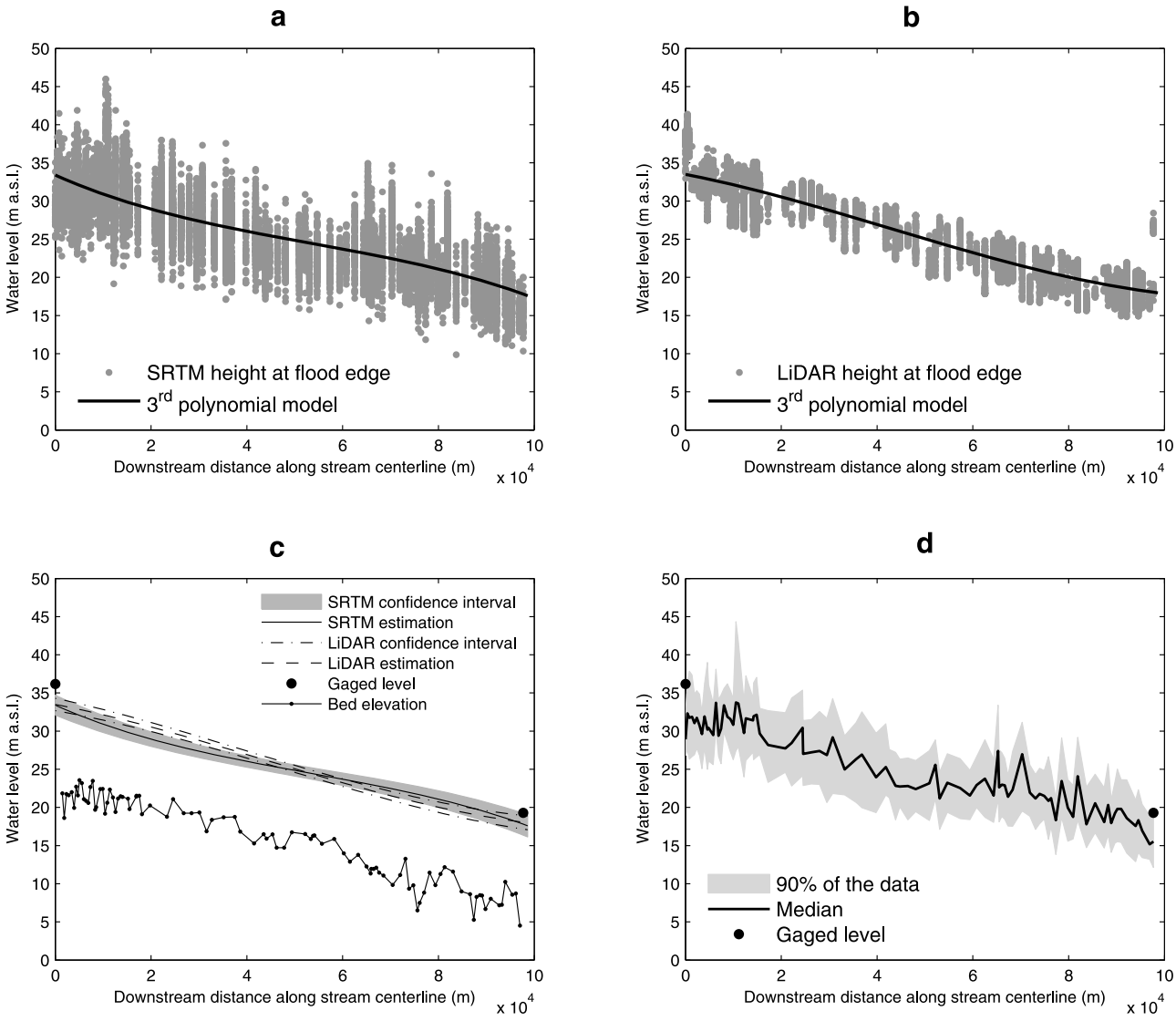

Figure 3. Flood water levels and wave approximation based on coarse resolution spaceborne remote sensing imagery with (a) the SRTM DEM and (b) the LiDAR DTM (note that we added no vertical error to the LiDAR DTM as it provided the reference data set). The approximation is given by a third-order polynomial. (c) A comparison between the SRTM-based flood wave approximation and that based on LiDAR, and (d) the distribution of possible SRTM-based water levels around the median.

where changes in topography have significant effects on the vertical accuracy of the SRTM DEM.

[24] The difference in gaged water levels between the upstream and downstream locations is 16.8 m over a distance of 98 km. The SRTM estimates 15.8 m as opposed to 15.5 m for the LiDAR. Although there is a difference of 2.76 m upstream between the SRTM and gaging station, conditioning the 3rd polynomial on the gaged water level upstream (36.18 m asl), as with hydraulic models, results in a difference of 19.4 m over the entire reach (gaged: 16.8), thus decreasing the reliability of the SRTM to estimate a reliable water surface gradient. An important point the authors wish to highlight is that regression modeling was only applied to compare the water surface gradient obtained with the SRTM to that of the LiDAR in the presence of processing uncertainties. If the aim is however to compare SRTM-derived water levels with those gaged or indeed a hydraulic model, we suggest to use the distribution of likely water levels from SRTM as shown in Figure 3d which illustrates that the gaged levels upstream (36.18 m asl) and downstream (19.29 m aal) fall inside the 90% range. There is only an 82 cm difference between the median estimate from SRTM and LiDAR.

[25] As a last validation step, we compare the SRTM water levels to those simulated by two HEC-RAS models with different parameterizations (see section 3.2 for full details). We expect this comparison to highlight the potential of water levels derived from low-resolution spaceborne image data to support hydraulic model calibration. Making use of the distribution of SRTM water levels, we defined a model acceptability target based on the 90% data range. For this range bounded by the 5th and 95th percentiles, it is sensible to accept a model that falls inside the range at 90% of all locations along the reach. Allowing a model to fail at 10% when omitting 10% of the data at each location seems a fair test. Figure 4 shows that the model calibrated on the high-magnitude event (HEC-RAS A) largely overestimates the

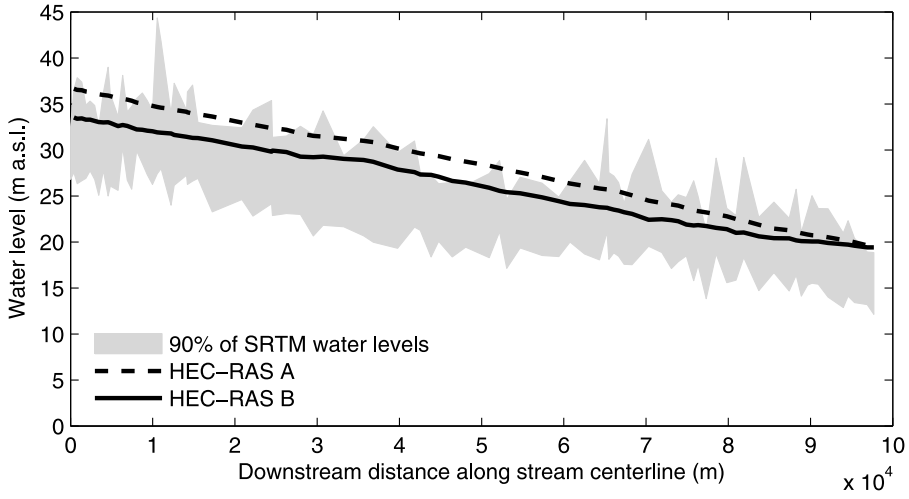

Figure 4. Comparison between SRTM-derived water levels and a hydraulic model of different parameterizations.

lower-magnitude event. Indeed, it falls inside the 90% range target only at 64% of locations. However, the recalibrated model for this event (HEC-RAS B) satisfies the target definition, with 90% of all locations. This suggests that low-resolution but more frequent spaceborne remote sensing could provide benchmark data for hydraulic models in the form of water levels or a flood wave gradient, albeit with difficulties of actually selecting the better model. In this context, it is worth noting that, for this site and event, instead of a recalibration of a 1-D model, a 2-D modeling approach might be preferred given that during this low-magnitude event floodplain dynamics were relevant once overtopping occurred.

[26] Our findings demonstrate that SRTM can be fused with low spatial resolution, high temporal frequency radar imagery to derive a reliable approximation of the water surface gradient and to compute estimates of possible water levels at maximum extent, provided that uncertainties are adequately accounted for. Even though results seem promising, in the context of distinguishing between different hydraulic model parameterizations the data are not without serious limitations. A caveat of accounting for horizontal uncertainties is of course that locating the flood edge close to the sideslopes of the floodplain will inevitably result in a significant skewness of the distribution thereby generating a hydraulically incoherent best estimate (median) water level. This effect is worsened by rapidly increasing height errors with even only moderate slope changes in topography in the case of lower-resolution DEMs, such as SRTM. Therefore it seems sensible to suggest that an error in flood edge positioning below the horizontal resolution of a lower-accuracy coarse resolution DEM is required if most flood edges are located close to higher slopes. Due to the combination of a low-magnitude inundation and the flat topography of the Po floodplain as well as a geolocation error below the SRTM resolution, this situation here did not occur. If however incoherences exist with regard to a smooth downward slope, the shape of the water level distributions along the reach should be examined. With the skewness measure, incoherent locations with a strong positive or negative skewness value can be omitted before putting the data to use. This might be particularly important for water level assimilation schemes that assume a normal distribution of the data, such as Ensemble Kalman filters.

6. Conclusions

[27] We have shown that globally and freely available low-resolution spaceborne data sets can be used to approximate the longitudinal profile of a flood wave on larger rivers in NRT. Intersecting scattered flood areas on a wide swath SAR image with the SRTM DEM generated a water surface gradient for the June 2008 flood on the River Po that is remarkably close to that derived when the SAR image is intersected with a high-resolution, high-accuracy LiDAR DEM. The SRTM-derived water profile data were shown to have significant value for the evaluation of hydraulic models, and were shown to be able to discriminate effectively between competing model parameterizations. This highlights that timely low-resolution spaceborne remote sensing of a flood event can be used to verify flood inundation models in near real time. The advantages of being able to use these data in this way are their greater spatial and temporal coverage, lower cost and lack of copyright restrictions. Confirmation of their utility therefore indicates the potential to remove an important obstacle currently preventing the routine application of hydraulic models to predict flood hazards globally, and potentially allows such technology to be extended to developing countries that have not previously been able to benefit from detailed flood predictions. The study also highlighted the potential utility for flood risk assessment of planned satellite missions, such as SWOT (see http://swot.jpl.nasa.gov/ and *Alsdorf et al.* [2007b]), that will measure flow width, water depth, and water slope changes globally at high temporal frequency with accuracies much higher than that achieved here. The SWOT mission may provide the beginning of a solution as over time high-accuracy repeat measurements of surface water elevation (at a nominal spatial resolution of about 30 m; height accuracies will be ±50 cm for individual pixels [*Alsdorf et al.*, 2007b], and thus decimetric accuracies are achieved through averaging methods) can be used to build up detailed floodplain topography maps using the so-called "waterline" method [*Mason et al.*, 1998]. With a maximum repeat time of ~10 days this potentially equates

to the retrieval of ~75 floodplain topographic contours over the scheduled 3 year SWOT mission lifetime [*Schumann et al.*, 2009], thereby yielding unprecedented detail concerning floodplain topography that can be used in inundation models.

[28] **Acknowledgments.** The authors are extremely grateful to the European Space Agency (ESA) for making the NRT image available through Category 1 (ID: 5752) and the River Po Basin Authority (Autorità di Bacino del Fiume Po, Italy) for the topographic and hydrologic data used in this study. Guy Schumann is funded by a Great Western Research fellowship, and part of Giuliano Di Baldassarre's time was funded by the FREE project of the Natural Environmental Research Council (NERC, grant NE/E002331/1). The authors wish to thank Jeffrey Neal and Timothy Fewtrell as well as three anonymous reviewers for their valuable suggestions and comments. Many thanks also go to the Associate Editor of this paper, Gregory Pasternack, for his very constructive review.

References

Alsdorf, D. E., J. M. Melack, T. Dunne, L. A. K. Mertes, L. L. Hess, and L. C. Smith (2000), Interferometric radar measurements of water level changes on the Amazon floodplain, *Lett. Nat.*, *404*, 174–177.

Alsdorf, D., P. Bates, J. Melack, M. Wilson, and T. Dunne (2007a), Spatial and temporal complexity of the Amazon flood measured from space, *Geophys. Res. Lett.*, *34*, L08402, doi:10.1029/2007GL029447.

Alsdorf, D. E., E. Rodriguez, and D. P. Lettenmaier (2007b), Measuring surface water from space, *Rev. Geophys.*, *45*, RG2002, doi:10.1029/2006RG000197.

Aronica, G., B. Hankin, and K. Beven (1998), Uncertainty and equifinality in calibrating distributed roughness coefficients in a flood propagation model with limited data, *Adv. Water Resour.*, *22*(4), 349–365.

Barkau, R. L. (1996), UNET: One-dimensional unsteady flow through a full network of open channels, user's manual, *Tech. Rep. 19961018082*, Hydrol. Eng. Cent., Davis, Calif.

Birkett, C. M., L. A. K. Mertes, T. Dunne, M. H. Costa, and M. J. Jasinski (2002), Surface water dynamics in the Amazon basin: Application of satellite radar altimetry, *J. Geophys. Res.*, *107*(D20), 8059, doi:10.1029/2001JD000609.

Blyth, K. (1997), Floodnet: A telenetwork for acquisition, processing and dissemination of Earth observation data for monitoring and emergency management of floods, *Hydrol. Processes*, *11*, 1359–1375.

Castellarin, A., G. Di Baldassarre, P. D. Bates, and A. Brath (2009), Optimal cross-section spacing in preissmann scheme 1D hydrodynamic models, *J. Hydraul. Eng.*, *135*, 96–105.

Di Baldassarre, G., G. Schumann, and P. Bates (2009), Near real time satellite imagery to support and verify timely flood modelling, *Hydrol. Processes*, *23*, 799–803.

European Environment Agency (2005), Vulnerability and adaptation to climate change: Scoping report, *Tech. Rep. 7*, Copenhagen, Denmark.

Falorni, G., V. Teles, E. R. Vivoni, R. L. Bras, and K. S. Amaratunga (2005), Analysis and characterization of the vertical accuracy of digital elevation models from the Shuttle Radar Topography Mission, *J. Geophys. Res.*, *110*, F02005, doi:10.1029/2003JF000113.

Farr, T. G., et al. (2007), The Shuttle Radar Topography Mission, *Rev. Geophys.*, *45*, RG2004, doi:10.1029/2005RG000183.

Frappart, F., K. Do Minh, J. L'Hermitte, A. Cazenave, G. Ramillien, T. Le Toan, and N. Mognard-Campbell (2006), Water volume change in the lower Mekong from satellite altimetry and imagery data, *Int. J. Geophys.*, *167*, 570–584.

Horritt, M. S., and P. D. Bates (2002), Evaluation of 1D and 2D numerical models for predicting river flood inundation, *J. Hydrol.*, *268*, 87–99.

Horritt, M. S., G. Di Baldassarre, P. D. Bates, and A. Brath (2007), Comparing the performance of a 2D finite element and a 2D finite volume model of floodplain inundation using airborne SAR imagery, *Hydrol. Processes*, *21*, 2745–2759.

Hostache, R., P. Matgen, G. Schumann, C. Puech, L. Hoffmann, and L. Pfister (2009), Water level estimation and reduction of hydraulic model calibration uncertainties using satellite SAR images of floods, *IEEE Trans. Geosci. Remote Sens.*, *47*, 431–441.

Jonkman, S. N., and J. K. Vrijling (2008), Loss of life due to floods, *J. Flood Risk Manage.*, *1*, 43–56.

Kiel, B., D. Alsdorf, and G. LeFavour (2006), Capability of SRTM C- and X-band DEM data to measure water elevations in Ohio and the Amazon, *Photogramm. Eng. Remote Sens.*, *72*, 313–320.

LeFavour, G., and D. Alsdorf (2005), Water slope and discharge in the Amazon river estimated using the shuttle radar topography mission digital elevation model, *Geophys. Res. Lett.*, *32*, L17404, doi:10.1029/2005GL023836.

Maione, U., P. Mignosa, and M. Tomirotti (2003), Regional estimation model of synthetic design hydrographs, *Int. J. River Basin Manage.*, *12*, 151–163.

Marcus, W. A., and M. A. Fonstad (2008), Optical remote mapping of rivers at sub-meter resolutions and watershed extents, *Earth Surf. Processes Landforms*, *33*, 4–24.

Mason, D. C., I. J. Davenport, R. A. Flather, and C. Gurney (1998), A digital elevation model of the inter-tidal areas of the Walsh, England, produced by the waterline method, *Int. J. Remote Sens.*, *19*(8), 1455–1460.

Mason, D. C., M. S. Horritt, J. T. Dall'Amico, T. R. Scott, and P. D. Bates (2007), Improving river flood extent delineation from Synthetic Aperture Radar using airborne laser altimetry, *IEEE Trans. Geosci. Remote Sens.*, *45*, 3932–3943.

Merz, B., A. H. Thieken, and M. Gocht (2007), Flood risk mapping at the local scale: Concepts and challenges, in *Flood Risk Management in Europe: Innovation in Policy and Practice (Advances in Natural and Technological Hazards Research)*, edited by S. Begum, M. J. F. Stive, and J. W. Hall, pp. 231–251, Springer, Dordrecht, Netherlands.

Ohl, C., and S. Tapsell (2000), Flooding and human health: the dangers posed are not always obvious, *Br. Med. J.*, *321*, 1167–1168.

Otsu, N. (1979), A threshold selection method from gray-level histograms, *IEEE Trans. Syst. Man Cybernetics*, *9*, 62–66.

Pappenberger, F., K. Beven, K. Frodsham, R. Romanowicz, and P. Matgen (2007), Grasping the unavoidable subjectivity in calibration of flood inundation models: a vulnerability weighted approach, *J. Hydrol.*, *333*, 275–287.

Pasternack, G. B., M. K. Bounrisavong, and K. K. Parikh (2008), Backwater control on riffle-pool hydraulics, fish habitat quality, and sediment transport regime in gravel-bed rivers, *J. Hydrol.*, *357*, 125–139.

Preissmann, A. (1961), Propagation of translatory waves in channels and rivers, paper presented at the First Congress of French Association for Computation, Grenoble, France.

Romanowicz, R., and K. J. Beven (2003), Estimation of flood inundation probabilities as conditioned on event inundation maps, *Water Resour. Res.*, *39*(3), 1073, doi:10.1029/2001WR001056.

Samuels, P. G. (1990), Cross section location in one-dimensional models, in *Proceedigns of International Conference on River Flood Hydraulics*, edited by W. R. White, pp. 339–350, John Wiley, Chichester, U. K.

Schumann, G., P. Matgen, F. Pappenberger, R. Hostache, and L. Pfister (2007), Deriving distributed roughness values from satellite radar data for flood inundation modelling, *J. Hydrol.*, *344*, 96–111.

Schumann, G., P. Matgen, M. E. J. Cutler, A. Black, L. Hoffmann, and L. Pfister (2008a), Comparison of remotely sensed water stages from LiDAR, topographic contours and SRTM, *J. Photogramm. Remote Sens.*, *63*, 283–296.

Schumann, G., P. Matgen, and F. Pappenberger (2008b), Conditioning water stages from satellite imagery on uncertain data points, *IEEE Geosci. Remote Sens. Lett.*, *5*, 810–813.

Schumann, G. J.-P., P. D. Bates, M. S. Horritt, P. Matgen, and F. Pappenberger (2009), Progress in integration of remote sensing derived flood extent and stage data and hydraulic models, *Rev. Geophys.*, *47*, RG4001, doi:10.1029/2008RG000274.

Shields, F. D., S. S. Knight, S. Testa, and C. M. Cooper (2003), Use of acoustic doppler current profilers to describe velocity distributions at the reach scale, *J. Am. Water Resour. Assoc.*, *39*, 1397–1408.

Smith, L. C. (1997), Satellite remote sensing of river inundation area, stage, and discharge: A review, *Hydrol. Processes*, *11*, 1427–1439.

U.S. Army Corps of Engineers (2002), Theoretical basis for one-dimensional flow calculations, in *Hydraulic Reference Manual*, version 3.1, pp. 2.1–2.38, Davis, Calif.

Wang, Y., M. Liao, G. Sun, and J. Gong (2005), Analysis of the water volume, length, total area and inundated area of the Three Gorges Reservoir, China using the SRTM DEM data, *Int. J. Remote Sens.*, *26*, 4001–4012.

Wilby, R. L., K. J. Beven, and N. S. Reynard (2008), Climate change and fluvial flood risk in the UK: More of the same?, *Hydrol. Processes*, *22*, 2511–2523.

D. Alsdorf, School of Earth Sciences, Ohio State University, Columbus, OH 43210, USA.

P. D. Bates and G. Schumann, School of Geographical Sciences, University of Bristol, University Road, Bristol BS8 1SS, UK. (guy.schumann@bristol.ac.uk)

G. Di Baldassarre, Department of Hydroinformatics and Knowledge Management, UNESCO-IHE, NL-2601 DA Delft, Netherlands.